ADVANCING EARTH AND SPACE SCIENCES

Geophysical Research Letters

RESEARCH LETTER

10.1029/2025GL116864

Electron Heat Fluxes for the Global Ionospheric Networks

George V. Khazanov[1], Viviane Pierrard[2,3], Mike Chu[4], and Edith Botek[2]

[1]NASA Goddard Space Flight Center, Greenbelt, MD, USA, [2]Royal Belgian Institute for Space Aeronomy, Solar-Terrestrial Center of Excellence (STCE) and Space Physics, Brussels, Belgium, [3]Université catholique de Louvain (UCLouvain), Earth and Life Institute - Climate Sciences (ELIC), Louvain-la-Neuve, Belgium, [4]The Space Weather Lab, George Mason University, Fairfax, VA, USA

Key Points:

- A new alternative approach for the calculation of electron heat fluxes using plasmaspheric modeling is presented
- The model shows strong electron heat flux variations at 800 km for variety of solar and magnetic activities
- The model also provides electron heating rate along the geomagnetic field lines between the southern and northern hemispheres

Correspondence to:

G. V. Khazanov,
George.V.Khazanov@nasa.gov

Citation:

Khazanov, G. V., Pierrard, V., Chu, M., & Botek, E. (2025). Electron heat fluxes for the global ionospheric networks. *Geophysical Research Letters*, *52*, e2025GL116864. https://doi.org/10.1029/2025GL116864

Received 5 MAY 2025
Accepted 2 JUL 2025

Abstract

This paper proposes an alternative approach for calculating electron heat fluxes by combining the Belgian 3D Plasmaspheric Model (Pierrard, Botek, & Darrouzet, 2021, https://doi.org/10.3389/fspas.2021.681401) and an analytical electron temperature formalism developed by Khazanov (2011), https://doi.org/10.1007/978-1-4419-6797-8. Such information is essential for 3D ionospheric modeling networks, which use the heat flux parameter as an upper boundary condition to calculate electron temperature, T_e, at altitudes below 700–800 km. The theoretical approach presented in this letter does not identify the nature of the magnetospheric cold electron temperature heating sources. Instead, it relies on the empirical thermal structure that is incorporated in the Belgian plasmasphere model and their calculation of total plasmaspheric cold plasma content. We also extended our results to plasmaspheric altitudes and provided cold electron heating rates along the geomagnetic field lines from the southern to the northern hemisphere for different magnetic and solar activities.

Plain Language Summary

Combining all possible electron heating sources of the cold plasma at the ionosphere-magnetosphere altitudes in single model to address the electron heat flux formation on the global scale is a very difficult task, and basically not achievable for the variety of solar and magnetospheric conditions. This letter offers an alternative method to reach this goal. Specifically, we combine the results of the Belgian plasmaspheric model and fundamental analytical relation between the electron temperature and electron thermal heat fluxes in single model and extract the thermal heat flux parameter for the broad range of magnetic, Kp = 1–6, and solar, $F_{10.7}$ = 70–250, activities.

1. Introduction

The heat or thermal electron fluxes play an important role in the calculation of the electron temperature, T_e, on the global scale (Bekerat et al., 2007; Glocer et al., 2012; Mishin, & Streltsov, 2021; Richmond et al., 1992; Ridley et al., 2006; Schunk et al., 1986) and are used in the ionospheric models as an upper boundary condition for the T_e calculations.

Electron thermal fluxes are coming from the plasmaspheric altitudes resulting from many different processes and can be classified as locally or non-locally formed (Khazanov, Chen, et al., 2023). The *locally formed* plasmaspheric heat fluxes related to high-energy magnetospheric particle are ring current (RC) protons (Cole, 1965), atomic oxygen (Khazanov et al., 2007; Kozyra et al., 1987). The hot plasma sheet electrons (Khazanov, 2011) also directly interacting with the cold background magnetospheric electrons via Coulomb collisions. Some magnetospheric waves participate in locally formed electron heat fluxes damping on the background electrons. Among them are ElectroMagnetic Ion Cyclotron (EMIC) (Cornwall et al., 1971; Khazanov et al., 2007), kinetic Alfven (Hasegawa & Mima, 1978), and lower hybrid (Khazanov, 2011; Mishin & Burke, 2005) waves.

The *non-locally formed* electron thermal fluxes are associated with photo- and secondary electrons production at ionospheric altitudes escaping to the plasmasphere and losing their energy via Coulomb collisions with thermal electrons (Khazanov, 2011; Schunk & Nagy, 2009). The whistler-mode waves (Khazanov, Ma, & Chu, 2022), Electron-Cyclotron Harmonic (ECH) (Khazanov et al., 2015; Ni et al., 2012), Time Domain Structures (TDSs) (Khazanov, Shen, et al., 2021; Shen et al., 2020) and other magnetospheric waves, mostly used for the RC and radiation belts (RB) dynamics studies, can also create the high-energy electron precipitation in the atmosphere and produce the secondary electron populations escaping to the magnetospheric altitudes actively interacting with cold plasmaspheric background thermal electrons. Through the magnetosphere-ionosphere-atmosphere (MIA) energy interplay, these waves that are not resonating directly with the thermal electrons, provide the non-local heating of cold plasmaspheric electrons.

Integrating all above-mentioned electron heating sources in single model to address electron heat flux formation is a challenging task and basically unfeasible for the variety of solar and magnetospheric conditions and global model availability of magnetospheric waves. This paper provides an alternative approach for calculating electron heat fluxes by combining the Belgian 3D Plasmaspheric Model (Pierrard, Botek, & Darrouzet, 2021) and the analytical electron temperature formalism developed by Khazanov (2011).

The twofold goal of this letter is to offer the ionospheric community global-scale heat flux calculations at 800 km altitudes and to provide the estimation of the cold electron heating rate along the closed geomagnetic field lines for the plasmaspheric global networks.

2. 3D Plasmasphere Model

2.1. General Overview

The Belgian SWIFF Plasmasphere-ionosphere Model (BSPM) (Pierrard, Botek, & Darrouzet, 2021) is a three dimensional dynamical model of the plasmasphere based on the kinetic approach, and constrained by empirical data for the convection electric field and for the coupling with the ionosphere (Pierrard & Voiculescu, 2011) using the IRI (International Reference Ionosphere) model (Bilitza et al., 2017). The particles of the plasmasphere are trapped in the terrestrial magnetic field (Pierrard & Stegen, 2008) until a sharp limit called the plasmapause that is determined at all magnetic local time (MLT) in the model by the interchange instability mechanism (Pierrard & Lemaire, 2004). The electric field combines the corotation field that dominates at low distance and the convection electric field that depends on the geomagnetic activity. By taking into account the 24-hr Kp history, the BSPM model can better capture the sudden geomagnetic storms and provides much more precisely the plasmapause at all MLT sectors than other simple linear functions relating a global plasmapause position to the maximum of Kp during the previous 24 hr, as explained in Pierrard, Botek, Ripoll, et al. (2021). The model allows us to determine the number density of the particles at any time inside the plasmasphere, and outside in the plasma trough where observations of the NASA RBSP satellites from 2012 to 2019 were used to determine the MLT and geomagnetic activity dependence (Botek et al., 2021). The results of the BSPM model have been validated against different physical processes (Bandic et al., 2020; Lemaire & Pierrard, 2008) and compared to many spacecraft observations: IMAGE (Pierrard & Stegen, 2008), Cluster (Verbanac et al., 2015), CRRES (Bandic et al., 2016), THEMIS (Verbanac et al., 2018) and Van Allen Probes (Pierrard, Botek, Ripoll, et al., 2021) among others. The electron, T_e, and ion, T_i, temperatures of the different ions are based on the IRI values up to 2,000 km, extended by empirical formulas at higher altitudes in the plasmasphere (Pierrard & Voiculescu, 2011). In the present work, the electron temperature of IRI is only used up to 800 km. The BSPM model can provide the plasmapause position and the particle density for past dates for which the geomagnetic activity indexes were observed, as well as for nowcasting or forecasting for space weather applications, as provided on the Space Situational Awareness (SSA) website of ESA (European Space Agency) (https://swe.ssa.esa.int/web/guest/bira-swiff-federated).

2.2. Logical Calculation Chain in BSPM

Figure 1a shows the electron number density obtained with the BSPM model (Pierrard, Botek, & Darrouzet, 2021) for two dates used in the simulations: 17 October 2018 at 3 hr UT (Universal Time) for low activity (two left panels) and 22 June 2015 at 17 hr UT for high activity (right panels).

The plasmasphere appears in orange tones, and the low-density plasma trough in green and blue. For each case, the plasmasphere is shown in the equatorial (left) and meridian (right) planes respectively. The plasmapause is represented by the black circles in the equatorial plane. The plasmasphere is extended and almost circular in the equatorial plane when the geomagnetic activity index of Bartels Kp is low (left) while a closer plasmapause with plumes is formed for higher activity, as already described. The Sun is located at 12 hr MLT to the left in the Figures.

In this letter, we consider nine cases with Kp = 1, 3 and 6 and $F_{10.7}$ = 70, 150 and 220–255 (see Figure 1b). Cases 1 and 9 correspond to those presented in Figure 1a. The datetimes have been chosen because they correspond approximately to these values. Because Kp is in fact not constant, the results depend not only on Kp itself, but also on its history during the previous 24 hr and thus depend on the date.

10.1029/2025GL116864

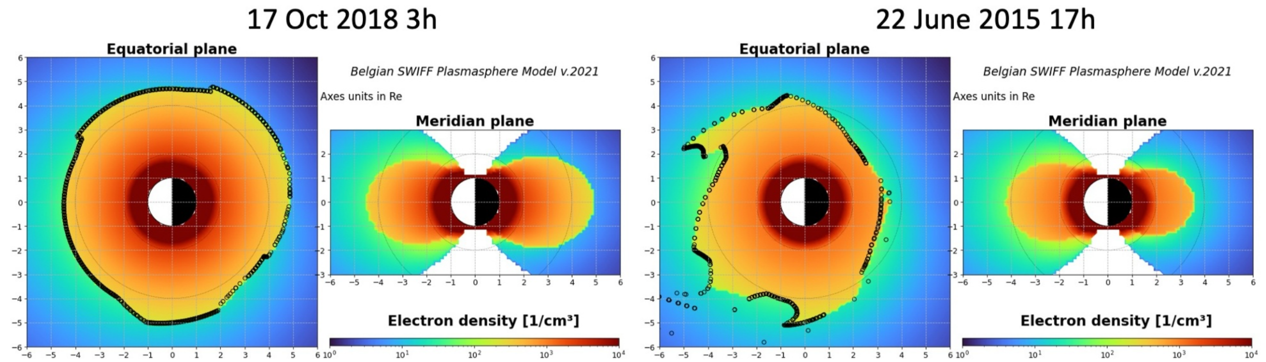

(a)

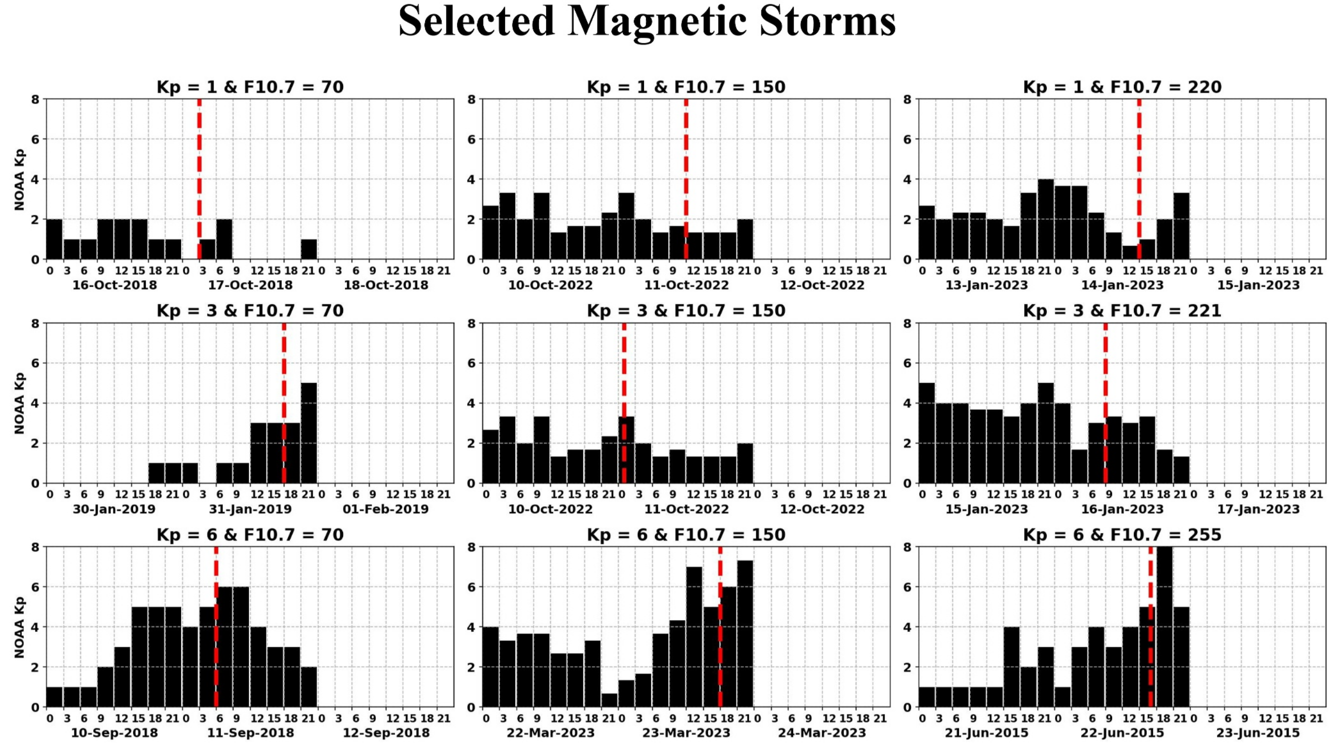

(b)

Figure 1. Panel (a). Electron density obtained with the BSPM model of the plasmasphere (Pierrard, Botek, & Darrouzet, 2021) in the equatorial and the meridian plane for low activity on 17 October 2018 at 3 hr UT (left panels) and high activity on 22 June 2015 at 17 hr UT (right panels). Panel (b) shows the evolution of the Kp index observed during the nine cases considered in this manuscript from low to high activity along with dates and solar and magnetic indexes.

3. Estimation of Electron Heat Fluxes From T_e Analytics

As it was previously demonstrated, the plasmaspheric cold electron content plays a fundamental role in the calculation of electron heat fluxes entering upper ionospheric altitudes (Khazanov, Ma, & Chu, 2022; Khazanov, Pierrard, et al., 2023). To support the ionospheric community with global-scale electron heat fluxes calculations and to estimate the electron heating rate along the closed geomagnetic field lines for the global plasmaspheric networks, we couple the BSPM model with the analytical formalism of T_e estimations presented in the books by Khazanov (1979, 2011).

Because the BSPM includes empirical plasmaspheric temperatures, it implicitly accounts for all potential energy sources mentioned in the introduction to this manuscript, within the spatial coverage locations of this plasmasphere model. To establish the heating sources for the thermal electrons, we first use the electron temperature equation at plasmaspheric altitudes. Above the altitude of 800 km, the energy balance of cold thermal electrons obeys the following equation (Khazanov, 2011; Chapter 6):

$$\frac{3}{2}kn_e(s)\frac{\partial T_e}{\partial s} = B(s)\frac{\partial}{\partial s}\left(\frac{k_e T_e^{\frac{5}{2}}}{B(s)}\frac{\partial T_e}{\partial s}\right) + Q_e(s), \tag{1}$$

where k is the Boltzmann constant, and $n_e(s)$ electron plasma density. The first term on the right hand side of Equation 1 represents the electron thermal conductance and the second one the electron heating rate along the geomagnetic field line at point s, with magnetic field of $B(s)$, and $k_e = 7.7 \cdot 10^5 \cdot T_e^{\frac{5}{2}}$ is a thermal conductivity in the units of $eV \cdot \mathrm{cm}^{-1} \cdot K^{-1} \cdot \mathrm{s}^{-1}$ (Banks, 1966).

On the time scale of the 3-hr Kp index, which drives the BSPM model, the time derivative in Equation 1 is neglected, as the formation of the electron heat flux occurs over much shorter time scales of a few minutes (Khazanov, Glocer, & Chu, 2021; Khazanov, Gabrielse, et al., 2022). Further, balancing the source term of Equation 1 with the divergence of the heat flux and integrating this equation along the field line from the geomagnetic equator to the upper ionospheric boundary, s_i, one can come up with the following relation, where Q_p is the energy content in the geomagnetic flux tube

$$q = \left(k_e T_e^{\frac{5}{2}}\frac{\partial T_e}{\partial s}\right)_{s_i} = \int_{s_{eq}}^{s_i} Q_e(s)\,\frac{B_i}{B(s)}ds = Q_p \tag{2}$$

Equation 2 corresponds to the thermal electron energy collected in the magnetosphere via multiple magnetospheric sources, $Q_e(s)$, with the thermal plasma. This energy transfers down to the ionosphere by thermal/heat electron energy flux of q to the upper ionospheric altitudes to define the electron temperature magnitude. One of the goals of our manuscript is to find this number. To do this, we assume that electron heating rate in Equation 2 can be presented as $Q_e(s) = a(s)\,n_e(s)$, where $a(s)$ is the electron heating rate per single thermal electron and $n_e(s)$ is the density of the thermal electrons along the field line (Khazanov, 2011).

Integrating Equation 2, the connection between the empirical electron temperature at lower boundary "*lb*"of BSPM simulation domain, 800 km, and the total cold plasma electron content in the magnetic field tube between the geomagnetic equator and the upper ionospheric boundary can be presented as

$$\frac{2k_e T_{e(lb)}^{\frac{7}{2}}}{7} = \overline{a}N_t \tag{3}$$

here, $T_{e(lb)}$ is the electron temperature at the lower boundary of BSPM simulation domain and N_t is the electron content of the magnetic flux tube content simulated by this model. The only unknown parameter in Equation 3 is $\overline{a}$ that represents the average electron heating rate per single thermal electron at plasmaspheric altitudes. By integrating the right-hand side of Equation 2, we assumed that this parameter changes much slower than the electron density, $n_e(s)$, along the field lines. This assumption is also consistent with the slow change of T_e(s) at plasmaspheric altitudes compared to the plasma field-aligned variations (Khazanov, 1979, 2011). The distribution of this parameter, $a(s)$, along the field lines is not critical, provided that the right-hand side integration value in Equation 2 remains unchanged. It is important to note that, in deriving Equation 3, no source of T_e heating is specified!

Besides the calculation of the heat fluxes on the global scale at the upper ionospheric altitudes, an additional goal of this paper is to obtain the electron heating rate at plasmaspheric altitudes. Previously, such an assessment was done for the photoelectron plasmaspheric heating source by Lejeune and Wormser (1976) based on the numerical solution of kinetic equation, and using the following approximation

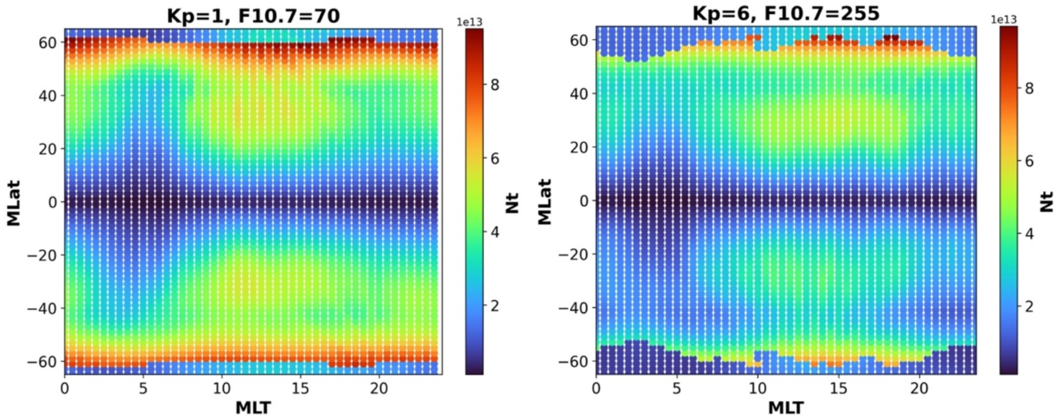

Figure 2. The total integral plasmaspheric content, N_t, as a function of the magnetic local time (MLT) and on the magnetic latitude (MLat) obtained by using the BSPM model of the plasmasphere for low activity on 17 October 2018 at 3 hr UT (case 1) and high activity on 22 June 2015 at 17 hr UT (case 9).

$$Q_e(s) = \frac{B(s)}{B_{\pm}(\pm s_i)} \frac{n_e(s)\, Q_p}{\int_{\pm s_i}^{s_{eq}} n_e(s)\, ds} \tag{4}$$

where Q_p is the total energy transferring to the thermal electron inside the half (northern or southern) part of geomagnetic field tube. Later such an approximation was confirmed analytically by Khazanov (2011, Chapter 5). We also analyzed the expression Equation 4 in the region of diffuse aurora that are driven by high energy electron precipitation and the production of secondary electrons through different magnetospheric wave-particle interaction processes (Khazanov, Glocer, & Chu, 2021; Khazanov & Chen, 2021; Khazanov, Ma, & Chu, 2022; Khazanov, Gabrielse, et al., 2022). In all above-mentioned cases, the expression Equation 4 is accurate within 15%–20% for their usage in the energy balance Equation 1 for the thermal electrons.

4. Global Electron Heat Fluxes and Field-Aligned Electron Heating Rates

The theoretical approach presented in the previous section does not identify the nature of magnetospheric cold electron temperature heating sources. Instead, it relies on the empirical thermal structure that is incorporated in the Belgian SWIFF Plasmasphere Model and on their calculations of total plasmaspheric cold plasma content that is shown in Figure 2 for two cases: lower (Kp = 1, $F_{10.7}$ = 70, 2018-10-17, 03:00:00) and higher (Kp = 6, $F_{10.7}$ = 255, 2015-06-22 17:00:00) geomagnetic and solar activities. This total plasmaspheric content, N_t, is coupled with the electron and ion temperatures for the solar and magnetic indexes, which serve as drivers of the model.

As it was demonstrated by Pierrard & Voiculescu (2011), inclusion of the empirical thermal structure in SWIFF model greatly improve modeling predictions for the plasmasphere during quiet and disturbed times. This is additional evidence of usefulness an alternative novel approach of heat flux calculation presented in this paper.

4.1. Heat Fluxes for Ionospheric Global Networks

Based on the information presented in Sections 2 and 3, we consider electron thermal fluxes, q and the average electron heating rate per single thermal electron, $\bar{a}$, for all cases we outlined in Figure 1b. These two parameters are presented together in Figure 3 and cover all the magnetic, Kp, and solar, $F_{10.7}$, indexes shown in Figure 1b. Among the nine cases considered in Figures 1b and 3, which represent different characteristics of geomagnetic and solar activities, four of them correspond approximately to solstice conditions, and the remaining five to the equinox dates. Interestingly, all cases exhibit enhanced thermal fluxes and elevated electron heating rate average per single thermal electron at the MLTs ~ 5–6. This reflects the empirical T_e feature at lower boundary of BSPM model when applying the corresponding parameters in Equations 2 and 3 relations. Such T_e behavior is consistent with the so-called "morning electron temperature overshoot," discovered a long time ago (Evans, 1965; Farley et al., 1967), and recently considered by Smirnov et al. (2025) during geomagnetic storms.

10.1029/2025GL116864

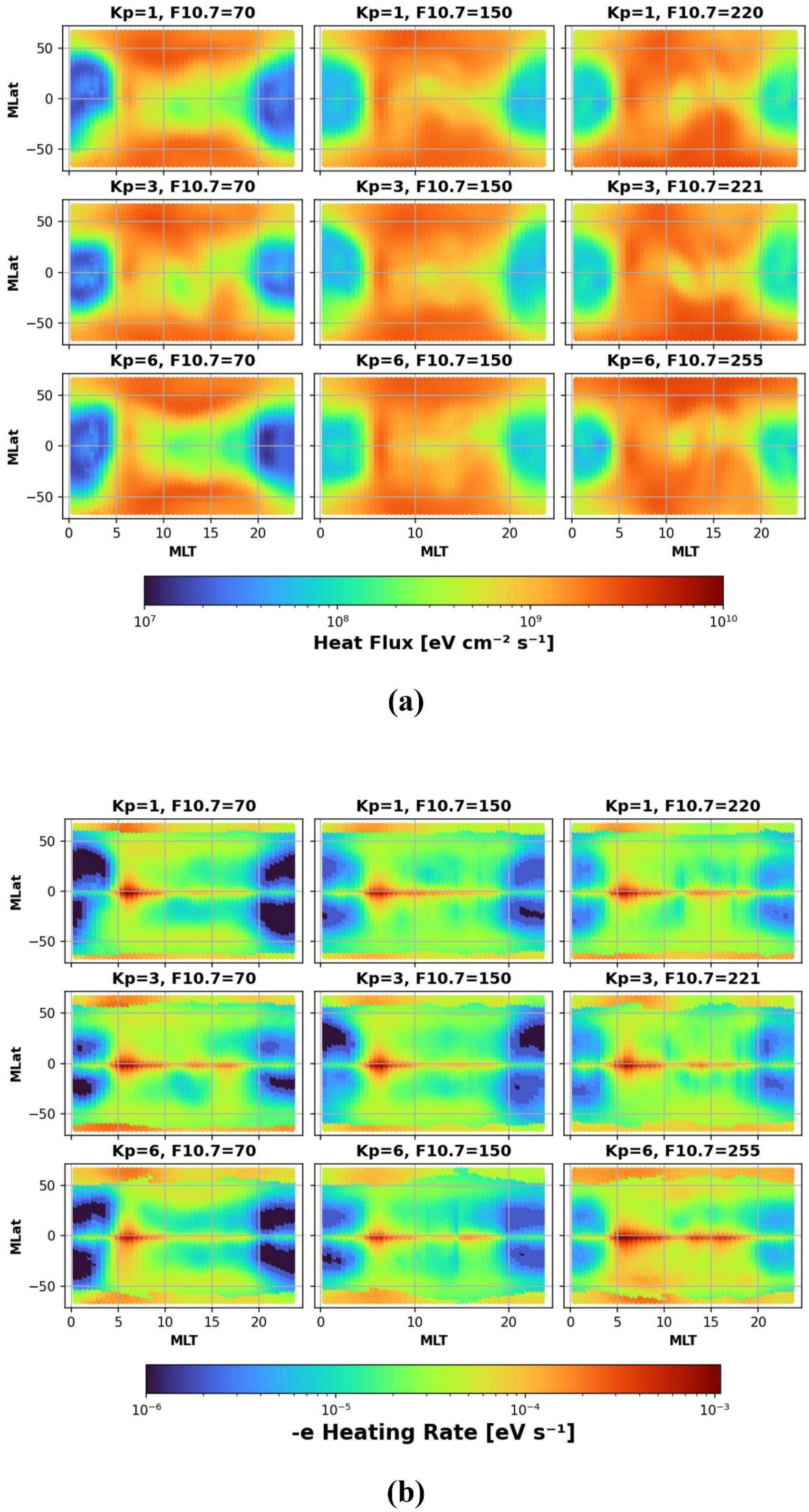

Figure 3. Electron heat/thermal fluxes (a) and average of electron heating rate per single thermal electron (b) at altitudes of 800 km as a function of MLT and MLat for the nine selected cases.

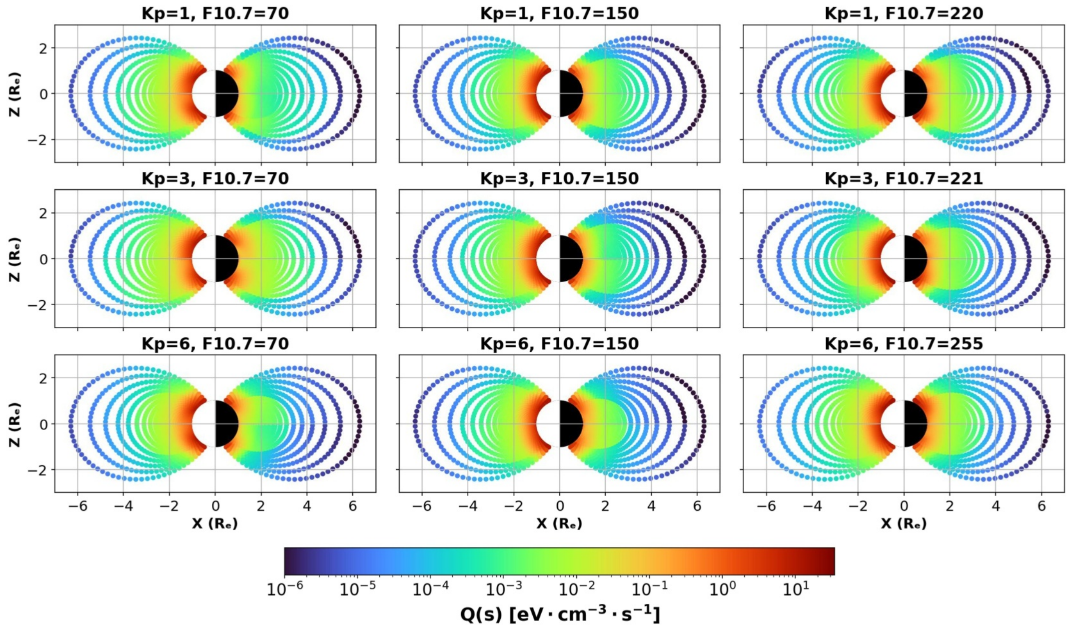

Figure 4. Field-aligned thermal electron heating rate at plasmaspheric altitudes and MLT = 0/12 for all nine selected cases of solar and magnetic activities presented in Figure 1b..

The equinox conditions (Kp = 1 & $F_{10.7}$ = 70; Kp = 1 & $F_{10.7}$ = 150; Kp = 3 & $F_{10.7}$ = 150; Kp = 6 & $F_{10.7}$ = 70 and Kp = 6 & $F_{10.7}$ = 150) for the parameters presented in Figure 3 are almost symmetric relative to MLT = 12 and MLat = 0 with clear visible day-night cutoffs at about ±30–45 MLat of the heat fluxes and electron heating rates representing the latitudinal range of differences of these parameters. This relates to the dominant role of solar activity in the latitudinal formation of the heat fluxes due to the escaping of ionospheric photoelectrons. At larger MLat ranges, other heating T_e mechanisms start to play a role, but the approach presented in this manuscript does not allow to identify specific physics of these processes.

Other combinations of Kp & $F_{10.7}$ parameters presented in Figure 3 correspond to the solstice dates and they clearly show the day-night and MLat north-south hemispheric asymmetries. These asymmetries are driven by both solar and magnetic processes and represent a variety of the physical mechanisms (see Introduction for details) involved in the formation of thermal electron fluxes and determined by T_e values at the upper ionospheric altitudes. Figure 3 presents both solstice and equinox dates, demonstrating how electron heat fluxes and electron heating rates spread across the MLT and MLat simulation domains. These parameters intensify with increasing solar ($F_{10.7}$) and magnetic (Kp) activity, reaching maximum values of $2–5 \times 10^9$ eV · cm^{-2} s^{-1} and 10^{-3}–10^{-4} eV/s, respectively. These numbers are consistent with first principal modeling of these parameters (Khazanov, 2011; Schunk & Nagy, 2009).

4.2. Field-Aligned Heating Rate for Plasmaspheric Models

As we have mentioned above, the major focus of our studies is offering to the ionospheric community the heat flux calculations on the global scale. Another goal of this work is an estimation of the cold electron heating rate along the closed geomagnetic field lines for the plasmaspheric global networks, as described by Equation 4. Figure 4 presents such a value on the global scale for all nine selected geomagnetic storms and solar activities that are shown in Figure 1b. Figure 4 clearly shows day-night asymmetry in the electron production rates along the geomagnetic field lines, but dependencies of these values on the characteristics of solar, $F_{10.7}$ index, and magnetic, Kp index, are not obvious, especially during the nighttime. Indeed, Pierrard and Lemaire (2004) and more recently Bandic et al. (2017) have clearly shown that the plasmapause is formed in the post-midnight sector depending on the Kp index observed at that time, while the plasmapause position at other MLTs depends on the Kp observed during the previous hours due to combination of corotation and convection. Because the geomagnetic activity (Kp index) given for the nine cases corresponds to a specific hour, the pre-midnight sector can correspond to other activity level. The selection of the specific datetimes is also a source of uncertainty, since

10.1029/2025GL116864

they correspond to the moment of specific geomagnetic activity, but the dynamics of the parameters can also be strongly influenced by the geomagnetic conditions of the previous 24 hr.

5. Discussion and Conclusion

The Earth's plasmasphere remains a crucial element in the ionospheric studies, as it provides the magnetospheric contribution to this region. The interaction with high-energy particles and plasma waves supplies particle and energy fluxes that maintain the upper ionosphere at the altitudes above the main maximum density in the F2 region (Lemaire & Gringauz, 1998; Schunk & Nagy, 2009). Simultaneously, the ionosphere is the source of the cold thermal plasmaspheric environment, refilling and reshaping this region via the quasi-neutral ionospheric outflows. Often the plasmasphere is considered as the extension of the ionosphere at low and mid-latitudes and is filled with low energy plasma (Lemaire & Gringauz, 1998), and the Belgian 3D plasmaspheric model by Pierrard, Botek, and Darrouzet (2021) uses a first-principles formalism for accounting all major dynamical physical processes that are involved in the formation of this region.

Knowledge of the thermal plasmaspheric structure, including the spatial and temporal distributions of electron and ion temperatures, is also a very critical element in studying this region. However, compared to plasma density distributions, these data are very limited and mostly rely on spacecraft observations (Kotova, 2007). As we discussed in the introduction, combining all possible electron heating sources of cold plasma at the ionosphere-magnetosphere altitudes into a single model present significant challenge. Addressing the plasmasphere energy structure formation and ionosphere-plasmasphere-magnetosphere energy interplay on the global scale is essentially not attainable for the variety of solar and magnetospheric conditions. Therefore, alternative approaches must be developed to address the connection of the ionosphere-plasmasphere thermal structure formation with the energy exchange between these two regions. This paper offers such an alternative, based on the combination of the Belgian 3D Plasmaspheric Model (Pierrard, Botek, & Darrouzet, 2021) and an analytical electron temperature formalism developed by Khazanov (2011).

The twofold goal of this letter is to offer to the ionospheric community global-scale heat flux calculations and provide the estimation of the cold electron heating rate along the closed geomagnetic field lines for the plasmaspheric global networks. This is accomplished without specifying the physical mechanisms responsible for the determination of the afore-mentioned values. It relates to temperature inclusion in the BSPM model that implicitly accounts for all potential energy sources mentioned in the introduction, at the locations covered by this plasmaspheric model.

At ionospheric altitudes, below approximately 800 km, electron and ion temperatures are strongly coupled with each other, and with electron and ion plasma densities (Schunk & Nagy, 2009). Thermal electrons serve as the heating source of the ions via Coulomb collisional processes, and ions provide electrons energy losses. At the plasmaspheric altitudes, however, Coulomb collisions between electron and ions greatly diminish, leaving thermal electrons effectively isolated and control their magnitude only by electron thermal conductivity and energy deposition processes. Ions at these altitudes still get energy from thermal electron-ion collision, but energy losses of the thermal electrons are mostly dependent on electron thermal conductivity process. Within the plasmasphere, these electrons gain energy from the interactions with high-energy particles and multiple plasma waves. They lose energy primarily due to thermal conductivity processes, which generate electron thermal fluxes at the upper ionospheric altitudes below 700–800 km. The data of INTERBALL mission and DMSP measurements show that at $L \sim 2.5$–2.8, ion temperatures in the plasmasphere are close to electron temperatures in the upper ionosphere everywhere except for the noon-to-dusk MLT sector (Kotova et al., 2008).

To simplify our approach, this letter focuses solely on thermal electron sources at plasmaspheric altitudes and excludes consideration of ion temperatures. Solving electron temperature equation in the plasmasphere in Section 3, we connected this analytical solution with BSPM, and further, in Section 4, considered electron heat fluxes for the global ionospheric networks and field-aligned electron heating rates for plasmaspheric models. The selected nine geomagnetic storms presented in Figure 1b span the broad range of the solar, $F_{10.7} = 70$–255, and geomagnetic conditions, Kp = 1–6. The resulting electron heat fluxes (Figure 3) and field-aligned electron heating rates (Figure 4) are presented and discussed on a global scale without attributing them to specific physical processes responsible for generating these practically important parameters.

To conclude our discussion, we must emphasize that we consider the approach presented in this letter as an alternative study of determination of heat/thermal fluxes, which largely depends on the quality of the empirical thermal structure incorporated in plasmaspheric models. Nevertheless, the results presented in this paper are pretty much consistent with the first-principles formalism considered in the past for specific plasmaspheric heating mechanisms (Khazanov, 2011; Khazanov et al., 2015, Khazanov, Shen, et al., 2021; Schunk & Nagy, 2009).

Data Availability Statement

The Belgian plasmasphere BSPM model used in the present article is made available at the CCMC Community Coordinated Modeling Center (https://ccmc.gsfc.nasa.gov/models/BSPM~2021/), at the ESA (European Space Agency) Virtual Space Weather Modeling Center (https://swe.ssa.esa.int/web/guest/bira-swiff-federated) and at PITHIA e-Science Center (https://esc.pithia.eu/data-collections/DataCollection_BSPM_2Dmaps/) through on-demand executions. The data heat flux obtained with the 3D ionospheric modeling networks presented in this paper are provided at Botek et al. (2025).

Acknowledgments

G. V. K. was partly supported MARBLE Project, funded by the NASA Living with a Star (LWS) Strategic Capabilities program and the Comprehensive Auroral Precipitation Experiment (CAPE) on NASA's Geospace Dynamics Constellation (GDC) mission as part of the LWS program. VP and EB thank (a) the project 21GRD02 BIOSPHERE that has received funding from the European Partnership on Metrology, co-financed by the European Union's Horizon Europe Research and Innovation Programme and by the Participating States, and (b) Horizon 2020 PITHIA-NRF with Grant agreement 101007599. The authors thank Joseph Lemaire for initiating plasmaspheric research at BIRA-IASB that led to the BSPM model.

References

Bandic, M., Verbanac, G., Moldwin, M., Pierrard, V., & Piredda, G. (2016). MLT dependence in the relationship between plasmapause, solar wind and geomagnetic activity based on CRRES: 1990-1991. *Journal of Geophysical Research*, *121*(5), 4397–4408. https://doi.org/10.1002/2015JA022278

Bandic, M., Verbanac, G., & Pierrard, V. (2020). Relationship between global plasmapause characteristics and plasmapause structures in the frame of interchange instability mechanism. *Journal of Geophysical Research: Space Physics*, *125*(2), e2019JA026768. https://doi.org/10.1002/2017JA024573

Bandic, M., Verbanac, G., Pierrard, V., & Cho, J. (2017). Evidence of MLT propagation of the plasmapause inferred from THEMIS data. *Journal of Atmospheric and Solar-Terrestrial Physics*, *161*, 55–63. https://doi.org/10.1016/j.jastp.2017.05.005

Banks, P. (1966). Charged particle temperatures and electron thermal conductivity in the upper atmosphere. *Annales Geophysicae*, *22*, 557–587.

Bekerat, H. A., Schunk, R. W., & Scherliess, L. (2007). Estimation of the highlatitude topside electron heat flux using DMSP plasma density measurements. *Journal of Atmospheric and Solar-Terrestrial Physics*, *69*(9), 1029–1048. https://doi.org/10.1016/j.jastp.2007.03.015

Bilitza, D., Altadill, D., Truhlik, V., Shubin, V., Galkin, I., Reinisch, B., & Huang, X. (2017). International reference ionosphere 2016: From ionospheric climate to real-time weather predictions. *Space Weather*, *15*(2), 418–429. https://doi.org/10.1002/2016SW001593

Botek, E., Pierrard, V., & Darrouzet, F. (2021). Assessment of the Earth's cold plasmatrough modeling by using Van Allen Probes/EMFISIS and Arase/PWE electron density data. *J. Geophys. Res.: Space Res.*, *126*(12), e2021JA029737. https://doi.org/10.1029/2021JA029737

Botek, E., Pierrard, V., & Khazanov, G. (2025). Electron heat fluxes for the global ionospheric networks: Dataset [Dataset]. *Zenodo*. https://doi.org/10.5281/zenodo.15674949

Cole, K. D. (1965). Stable auroral red arcs, sinks for energy of Dst main phase. *Journal of Geophysical Research*, *70*(7), 1689–1706. https://doi.org/10.1029/JZ070i007p01689

Cornwall, J. M., Coroniti, F. V., & Thorne, R. M. (1971). Unified theory of SAR arc formation at the plasmapause. *Journal of Geophysical Research*, *76*(19), 4428–4445. https://doi.org/10.1029/JA076i019p4428

Evans, J. V. (1965). Cause of the midlatitude evening increase in f oF2. *Journal of Geophysical Research*, *70*, 1175–1185. https://doi.org/10.1029/JZ070i017p04331

Farley, D. T., McClure, J. P., Sterling, D. L., & Green, L. J. (1967). Temperature and composition of the equatorial ionosphere. *Journal of Geophysical Research*, *72*(23), 5837–5851. https://doi.org/10.1029/JZ072i023p05837

Glocer, A., Kitamura, N., Toth, G., & Gombosi, T. (2012). Modeling solar zenith angle effects on the polar wind. *Journal of Geophysical Research*, *117*(A4), A04318. https://doi.org/10.1029/2011JA017136

Hasegawa, A., & Mima, K. (1978). Anomalous transport produced by kinetic Alfven wave turbulence. *Journal of Geophysical Research*, *83*(A3), 1117–1123. https://doi.org/10.1029/JA083iA03p01117

Khazanov, G. (1979). *The kinetics of the electron plasma component of the upper atmosphere*. Nauka.

Khazanov, G. V. (2011). Kinetic theory of inner magnetospheric plasma. In *Astrophysics and space science library* (Vol. 372, p. 584). Springer Science & Business Media.

Khazanov, G. V., & Chen, M. W. (2021). Why atmospheric backscatter is important in the formation of electron precipitation in the diffuse aurora. *Journal of Geophysical Research: Space Physics*, *126*(5), e2021JA029211. https://doi.org/10.1029/2021JA029211

Khazanov, G. V., Chen, M. W., Mishin, E. V., & Chu, M. (2023). Thermal electron heat fluxes associated with precipitated auroral electrons during the Saint Patrick's Days 2013 and 2015 geomagnetic storms. *Journal of Geophysical Research: Space Physics*, *128*(2), e2022JA031197. https://doi.org/10.1029/2022JA031197

Khazanov, G. V., Gabrielse, C., Glocer, A., Chu, M., Nishimura, Y., & Reyes, P. (2022). A 2D kaleidoscope of electron heat fluxes driven by auroral electron precipitation. *Geophysical Research Letters*, *49*(18), e2022GL100912. https://doi.org/10.1029/2022GL100912

Khazanov, G. V., Gamayunov, K. V., Gallagher, D. L., Kozyra, J. U., & Liemohn, M. W. (2007). Self-consistent model of magnetospheric ring current and propagating electromagnetic ion cyclotron waves: 2. Wave-Induced ring current precipitation and thermal electron heating. *Journal of Geophysical Research*, *112*(A4), A04209. https://doi.org/10.1029/2006JA012033

Khazanov, G. V., Glocer, A., & Chu, M. (2021). Electron energy interplay in the geomagnetic trap below the auroral acceleration region. *Journal of Geophysical Research: Space Physics*, *126*(5), e2020JA028811. https://doi.org/10.1029/2020JA028811

Khazanov, G. V., Ma, Q., & Chu, M. (2022). Electron heat fluxes generated by intense whistler waves at the upper ionospheric altitudes. *Journal of Geophysical Research: Space Physics*, *127*(9), e2022JA030753. https://doi.org/10.1029/2022JA030753

Khazanov, G. V., Pierrard, V., Ma, Q., & Botek, E. (2023). The role of plasmasphere in the formation of electron heat fluxes. *Journal of Geophysical Research: Space Physics*, *128*(11), e2023JA032013. https://doi.org/10.1029/2023JA032013

Khazanov, G. V., Shen, Y., Vasko, I. Y., Artemyev, A. V., & Chu, M. (2021). Magnetosphere-ionosphere coupling of precipitated electrons in diffuse aurora driven by time domain structures. *Geophysical Research Letters*, *48*(10), e2021GL092655. https://doi.org/10.1029/2021GL092655

Khazanov, G. V., Tripathi, A. K., Sibeck, D., Himwich, E., Glocer, A., & Singhal, R. P. (2015). Electron distribution function formation in regions of diffuse aurora. *Journal of Geophysical Research: Space Physics*, *120*(11), 9891–9915. https://doi.org/10.1002/2015JA021728

Kotova, G. (2007). The Earth's plasmasphere: State of studies (a Review). *Geomagnetism and Aeronomy*, *47*(4), 409–422. https://doi.org/10.1134/s0016793207040019

Kotova, G., Bezrukikh, V., Verigin, M., & Smilauer, J. (2008). New aspects in plasmaspheric ion temperature variations from INTERBALL 2 and MAGION 5 measurements. *Journal of Atmospheric and Solar-Terrestrial Physics*, *70*(2–4), 399–406. https://doi.org/10.1016/j.jastp.2007.08.054

Kozyra, J. U., Shelley, E. G., Comfort, R. H., Brace, L. H., Cravens, T. E., & Nagy, A. F. (1987). The role of ring current O^+ in the formation of stable auroral red arcs. *Journal of Geophysical Research*, *92*(A7), 7487–7502. https://doi.org/10.1029/JA092iA07p07487

Lejeune, J., & Wormser, F. (1976). Diffusion of photoelectrons along a field line inside the plasmasphere. *Journal of Geophysical Research*, *81*(16), 2900–2916. https://doi.org/10.1029/ja081i016p02900

Lemaire, J., & Gringauz, K. I. (1998). *The Earth's plasmasphere*. Cambridge University Press. https://doi.org/10.1017/CBO9780511600098

Lemaire, J., & Pierrard, V. (2008). Comparison between two theoretical mechanisms for the formation of the plasmapause and relevant observations. *Geomagnetism and Aeronomy*, *48*(5), 553–570. https://doi.org/10.1134/S0016793208050010

Mishin, E., & Burke, W. (2005). Stormtime coupling of the ring current, plasmasphere and topside ionosphere: Electromagnetic and plasma disturbances. *Journal of Geophysical Research*, *110*(A7), A07209. https://doi.org/10.1029/2005JA011021

Mishin, E. V., & Streltsov, A. (2021). *Nonlinear wave and plasma structures in the auroral and subauroral geospace* (p. 621). Elsevier.

Ni, B., Liang, J., Thorne, R. M., Angelopoulos, V., Horne, R. B., Kubyshkina, M., et al. (2012). Efficient diffuse auroral electron scattering by electrostatic electron cyclotron harmonic waves in the outer magnetosphere: A detailed case study. *Journal of Geophysical Research*, *117*(A1), A01218. https://doi.org/10.1029/2011JA017095

Pierrard, V., Botek, E., & Darrouzet, F. (2021). Improving predictions of the 3D dynamic model of the plasmasphere. *Front. Astron. Space Sci.*, *8*, 681401. https://doi.org/10.3389/fspas.2021.681401

Pierrard, V., & Lemaire, J. (2004). Development of shoulders and plumes in the frame of the interchange instability mechanism for plasmapause formation. *Geophysical Research Letters*, *31*(5), L05809. https://doi.org/10.1029/2003GL018919

Pierrard, V., & Stegen, K. (2008). A three-dimensional dynamic kinetic model of the plasmasphere. *Journal of Geophysical Research*, *113*(A10), A10209. https://doi.org/10.1029/2008JA013060

Pierrard, V., & Voiculescu, M. (2011). The 3D model of the plasmasphere coupled to the ionosphere. *Geophysical Research Letters*, *38*(12), L12104. https://doi.org/10.1029/2011GL047767

Pierrard, V. E., Botek, J.-F., Ripoll, S. A., Thaller, M. B., Moldwin, M., Ruohoniemi, G., & Reeves, G. (2021). Links of the plasmapause with other boundary layers of the magnetosphere: Ionospheric convection, radiation belts boundaries, auroral oval. *Frontiers in Astronomy and Space Sciences*, *8*, 728531. https://doi.org/10.3389/fspas.2021.728531

Richmond, A. D., Ridley, E. C., & Roble, R. G. (1992). A thermosphere/ionosphere general circulation model with coupled electrodynamics. *Geophysical Research Leterrs*, *19*(6), 601–604. https://doi.org/10.1029/92gl00401

Ridley, A. J., Deng, Y., & Toth, G. (2006). The global ionosphere–thermosphere model. *Journal of Atmospheric and Solar-Terrestrial Physics*, *68*(8), 839–864. https://doi.org/10.1016/j.jastp.2006.01.008

Schunk, R. W., & Nagy, A. F. (2009). *Ionospheres: Physics, plasma physics, and chemistry*. Cambridge University Press.

Schunk, R. W., Sojka, J. J., & Bowline, M. D. (1986). Theoretical study of the electron temperature in the high-latitude ionosphere for solar maximum and winter conditions. *Journal of Geophysical Research*, *91*(A11), 12041–12054. https://doi.org/10.1029/JA091iA11p12041

Shen, Y., Artemyev, A., Zhang, X. J., Vasko, I. Y., Runov, A., Angelopoulos, V., & Knudsen, D. (2020). Potential evidence of low-energy electron scattering and ionospheric precipitation by time domain structures. *Geophysical Research Letters*, *47*(16), e2020GL089138. https://doi.org/10.1029/2020GL089138

Smirnov, A., Shprits, Y., Lühr, H., Pignalberi, A., Kronberg, E., Prol, F., & Xiong, C. (2025). Extreme two-phase change of ionospheric electron temperature overshoot during geomagnetic storms. *Scientific Reports*, *15*(1), 5043. https://doi.org/10.1038/s41598-025-89602-z

Verbanac, G., Bandic, M., & Pierrard, V. (2018). MLT plasmapause characteristics: Comparison between THEMIS observations and numerical simulations. *Journal of Geophysical Research: Space Physics*, *123*, 2000–2017. https://doi.org/10.1002/2017JA024573

Verbanac, G., Pierrard, V., Bandic, M., Darrouzet, F., Rauch, J.-L., & Décréau, P. (2015). Relationship between plasmapause, solar wind and geomagnetic activity between 2007 and 2011 using Cluster data. *Annales Geophysicae*, *33*, 1271–1283. https://doi.org/10.5194/angeo-33-1271-2015